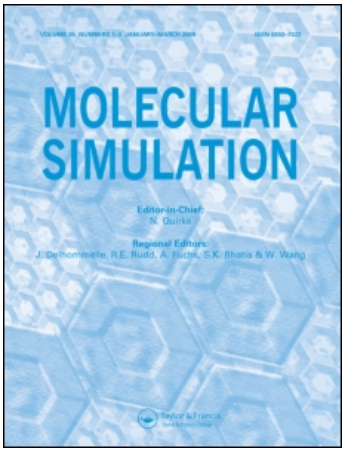

Molecular Simulation
Publication details, including instructions for authors and subscription information:
http://www.informaworld.com/smpp/title~content=t713644482

Coupling of Penetrant and Polymer Motions During Small-Molecule Diffusion In a Glassy Polymer

Michael L. Greenfield[ab]; Doros N. Theodorou[c]
[a] Department of Chemical Engineering, University of California, Berkeley, CA [b] Ford Research Laboratory, Ford Motor Company, Dearborn, MI [c] Department of Chemical Engineering, University of Patras and ICE/HT-FORTH, Patras, Greece

To cite this Article Greenfield, Michael L. and Theodorou, Doros N.(1997) 'Coupling of Penetrant and Polymer Motions During Small-Molecule Diffusion In a Glassy Polymer', Molecular Simulation, 19: 5, 329 — 361
To link to this Article: DOI: 10.1080/08927029708024161
URL: http://dx.doi.org/10.1080/08927029708024161

Molecular Simulation, 1997, Vol. 19, pp. 329–361
Reprints available directly from the publisher
Photocopying permitted by license only

COUPLING OF PENETRANT AND POLYMER MOTIONS DURING SMALL-MOLECULE DIFFUSION IN A GLASSY POLYMER

MICHAEL L. GREENFIELD[a,†] and DOROS N. THEODOROU[b,*]

[a]*Department of Chemical Engineering, University of California, Berkeley, Berkeley, CA 94720;* [b]*Department of Chemical Engineering, University of Patras and ICE/HT-FORTH, P.O. Box 1414, GR 26500 Patras, Greece*

(Received February 1997; Accepted February 1997)

Multidimensional transition-state theory was used to simulate methane jump motions in glassy atactic polypropylene at 233 K in the limit of small methane concentrations. Transition states were found with respect to both penetrant and polymer degrees of freedom, using all generalized coordinates associated with atoms interacting with the methane penetrant. Animations followed the multidimensional reaction coordinate for three different jumps.

The jump mechanism involved polymer atoms retracting to form a channel, followed by penetrant motion through the channel. Methyl groups within 4 Å of the penetrant transition state location were displaced by 0.9 Å on average, while carbon atoms and methyl groups further than 9 Å from the penetrant transition state location were displaced by less than 0.2 Å.

The energy profiles along the diffusion path differed considerably among all jumps simulated, and the jump rate did not correlate simply with changes in particular types of degrees of freedom. Jumps for which the penetrant transition state location was within 5 Å of a chain start or end had average rates of order 60 μs^{-1}, while jumps further from a chain start or end were an order of magnitude slower.

Keywords: Glassy polymer; gas diffusion; atactic polypropylene; transition-state theory

1. INTRODUCTION

Numerous products and processes succeed or fail due to the diffusion of small- to moderate-size molecules within glassy polymers. Various phenomenological theories exist for interpreting and correlating experimental

*To whom correspondence should be addressed.
†Present address: Ford Research Laboratory, Ford Motor Company, P.O. Box 2053, Mail Drop 3083/SRL, Dearborn, MI 48121-2053.

diffusion measurements, which are made as functions of temperature, concentration, and/or diffusing species [1]. Phenomenological models are useful in engineering design and assessment, since they are parameterized reliably over ranges of interest. However, their utility diminishes for new materials and/or systems, since the parameters that would ensure an appropriate concellation of errors are not known.

Most phenomenological models of penetrant diffusion in polymers fall in three classes: the molecular, free volume, and dual-mode models. The molecular theories of Brandt [2] and of Pace and Datyner [3–5] presuppose particular molecular mechanisms for diffusion and obtain a diffusion coefficient from the associated energetics. The predicted activation energy is of the correct order of magnitude, but the jump length that results (of order 10–50 nm) is significantly longer than the molecular length scale of channels and voids in glassy polymers. The free-volume theories of Vrentas and Duda [6–8] predict the concentration dependence of the penetrant diffusivity. Some parameters, such as the specific volume at 0 K, are well defined, while others, such as the free-volume parameters for the solvent and polymer and the ratio of molar volumes for the jumping units, cannot be interpreted clearly on the molecular level and are only defined by other empirical correlations [9]. The dual-mode transport model [10–13] builds upon the dual-mode sorption model [14, 15] by incorporating different transfer rates between the two types of sorption states. The resulting equations for the temperature and concentration dependence of the diffusivity correlate experimental data very well [1]. However, numerous experiments have either failed to observe two populations of sites or have detected significant interactions between the diffusing species and the host polymer [16, 17]. Other experiments were interpreted by invoking a broad distribution of site energies and jump rates [18]. While some experiments have claimed to support dual-mode interpretations [19, 20], many assumptions about the underlying behavior were invoked, and the large number of accompanying parameters complicates the analysis.

One general problem with phenomenological approaches is that the molecular mechanisms are assumed, rather than inferred. Without firsthand knowledge of such information, extensions to new materials rely on rules of thumb, which are often valid, but not always. The roles of molecular simulations in this area are to address the deficiencies of the phenomenological models, to elucidate the qualitative aspects of the molecular diffusion mechanism, and, to a lesser extent, to determine quantitative values of the diffusion coefficient for particular penetrant–polymer combinations. Two reviews discussing the molecular simulation of small molecule diffusion in

amorphous polymers have appeared recently [21, 22]. Most investigators have used molecular dynamics (MD). The success of this method relies on sufficiently fast penetrant diffusion, as is found in a polymer melt. MD simulations in the glass and at temperatures slightly above the glass transition have elucidated an important mechanistic aspect of diffusion: slight fluctuations in the polymer configuration infrequently open a pathway between the location of the penetrant and another sorption site. This allows the penetrant to move or hop between sites, as shown pictorially by Takeuchi for oxygen in polyethylene [23], by Sok *et al.* for methane in poly(dimethyl siloxane) [24], and by Müller-Plathe *et al.* for oxygen in polyisobutylene [25]. In a glassy polymer, these jumps are rare events, and they occur too infrequently to be properly sampled with MD. Most simulation time is spent detailing the rattling motions within a sorption site, and jumps only occur occasionally.

The separation of time scales (between rattling and hopping) necessitates more coarse-grained approaches. Suter and co-workers have used transition-state theory to study the hopping motions of small penetrants in both glassy and melt polymers. Sorption sites were identified as local minima on the three-dimensional potential energy hypersurface imposed on the penetrant by the polymer. Arizzi [26] considered helium, oxygen, and nitrogen diffusion between tetrahedral interstices in static and fluctuating structures of atactic polypropylene and glassy bisphenol-A polycarbonate. In static structures he used two different expressions for the rate constant. Using a specified frequency prefactor, the predicted diffusivity was two orders of magnitude too high. In fluctuating structures and in static structures with a prefactor determined with a harmonic approximation, the predicted diffusivity was closer to the experimental value. The structures were fluctuated using a version of the method published by Gusev and Suter. Gusev *et al.* [21, 27–29] considered penetrant diffusion through glassy and melt polyisobutylene and polycarbonate. First, they assumed that the polymer was static [27]. High energy barriers were found between sorption sites and the predicted diffusivity was much smaller than 10^{-12} cm^2sec^{-1} for gases other than helium. Next, Gusev and Suter considered penetrant diffusion in a polymer whose atoms vibrated harmonically and independently about their equilibrium positions [28]. The amplitude of the position fluctuations was a parameter extracted from short-time MD simulations. This description corresponded to diffusion on an imposed free energy hypersurface. For the systems under consideration, the predicted and experimental diffusivities agreed within an order of magnitude. However, the amplitude of harmonic vibrations was essentially an adjustable parameter, and the sensitivity of the diffusion coefficient to that parameter

was not clear. Gusev *et al.* presented a method of evaluating it self-consistently, based on the average residence time a penerant spends in a cavity [28]. Although economic computationally, the Gusev *et al.* TST approach disregards direct couplings between polymer and penetrant motions, which may be important for larger penetrants, such as alkanes and aromatics. Both their implementations used three-dimensional transition-state theory, with the polymer degrees of freedom remaining constant or contributing to an elastic free energy felt by the penetrant.

We have developed methods that complement the transition-state theory-based approach of Gusev and Suter. The barriers for penetrant jumps are approximated with transition-state theory, but the transition states and diffusion paths are defined with respect to the penetrant position *and* the local polymer chain conformation. Changes in polymer conformation are included explicitly along the diffusion path. A description of the method itself has appeared in a limited form [30–32]. The goal of this paper in particular is to extract information about the molecular-level polymer chain processes that accompany isolated methane hops within an amorphous matrix of glassy atactic polypropylene. This work is part of a larger effort on our part [31, 32] to simulate small-molecule diffusion in a glassy polymer using multidimensional transition-state theory.

2. MODEL AND SIMULATION METHOD

This work was based on a model of polypropylene originally developed by Suter and Flory [33] and extended to bulk systems by Theodorou and Suter [34]. As in those works, polypropylene was modeled classically, using a collection of atomic-level microstructures to represent the variety of conformations found in a glassy sample of unknown preparation history. Each microstructure contains three ($N_{ch} = 3$) 50-unit atactic polypropylene chains (MW = 2120 g mol^{-1}) packed into a cube with edge lengths 22.79 Å, corresponding to the experimental density of 0.892 g cm^{-3} at 233 K, 1 atm [34]. A single methane molecule ($N_{pen} = 1$) was considered within each polymer microstructure. Periodic boundary conditions were used to prevent surface effects [35]. The combination of methane and atactic polypropylene was chosen because of its chemical simplicity, allowing us to concentrate on the details of the method. The methods used for generating each polymer microstructure are discussed below.

The polypropylene model used here is a hybrid between a fully explicit model and a "united-atom" model. Backbone carbon atoms were treated

explicitly, as were pendant hydrogen atoms. Chain starts, chain ends, and pendant methyl groups were treated as (CH_3) united atoms. The methane penetrant was represented as a single spherical site. Within each microstructure, the three-dimensional locations of all atoms on each chain were calculated from a set of generalized coordinates: the chain start position, Eulerian angles (which define the chain orientation), bond lengths, bond angles, and torsion angles. Definitions for these coordinates were taken from Ref[34]. Bond lengths remained fixed throughout the simulations. Backbone C-C-C and pendant C-C-R and R-C-C angles — unlike in Ref[34] – remained flexible: they were allowed to fluctuate during the course of the simulations.

In a previous investigation of an atactic polypropylene free surface [36], it was found that the H-C-H angle vibrated at high frequencies, which were computationally expensive to track and were not well described in a classical framework. To eliminate the need to treat the H-C-H vibration in this work, the positions of the hydrogen atoms were expressed in terms of the positions of the backbone carbon atoms and the pendant methyl groups. The H-C-H, H-C-C, and H-C-R bond angles were *not* considered degrees of freedom in this representation.

This separate treatment of hydrogen atoms results in two classes of atoms. The primary atoms are those that define the chain position and conformation – backbone carbon atoms and pendant methyl groups. The secondary atoms are those whose positions depend on the positions of the primary atoms – i.e., the hydrogen atoms. The superset of these two sets is the full representation, which was the model of polypropylene used in the works cited above. In other words, there are a total of $N=6\times50-1=299$ interaction sites or "atoms" per polypropylene chain.

Both primary and secondary atoms were retained as centers of force. For tracking the system evolution with classical molecular dynamics, however, hydrogen atoms were considered to have zero mass. Instead, their mass was added to the backbone carbon to which they were bound. Three different masses were used for carbon groups. Chiral and achiral backbone carbons were assigned masses of 13 and 14 AMU, respectively. Each pendant methyl group, lumped into a single united atom, was assigned a mass of 15 AMU.

The total potential energy of a particular penetrant–polymer configuration

$$\mathcal{V} = \mathcal{V}^{\theta} + \mathcal{V}^{\phi} + \mathcal{V}^{\text{pen}} + \mathcal{V}^{nb} \tag{1}$$

was found as a sum of four individual terms. All potential energy parameters are listed in Table I. Bond lengths were considered flexible in

the limit of infinite stiffness [37] and did not contribute to differences in energy among different configurations. Bond angles along the chain backbone and between the backbone and pendant methyl groups contributed a three-body term

$$\mathcal{V}^{\theta} = \sum_{i} k_{\theta}(\theta_i - \theta_{i0})^2 \tag{2}$$

to the total potential energy. Parameters were taken from work by Sylvester *et al.* [38]. The values of k_θ and θ_{i0} depend on the bond angle considered.

TABLE I Potential energy parameters used in the simulations. Polymer parameters are taken from Refs [34, 38]. Penetrant parameters are taken from Ref [42].
Slater-Kirkwood nonbonded interaction parameters

type	r_{vdW} (Å)	$\alpha/4\pi\epsilon_0$ (Å^3)	n_e	*mass(AMU)*
H	1.3	0.42	0.9	1.00
C	1.8	0.93	5.0	13.00, 14.00*
CH_3	2.0	1.77	7.0	15.00

r_{vdW}: van der Waals radius
α: polarizability
n_e: effective number of electrons
*masses of chiral and achiral units, respectively

Resulting equivalent Lennard-Jones parameters and cutoff distances:

species i	*species j*[*,†]	$\varepsilon_{i,j}$ (kcal/mol)	σ_{ij} (Å)	*cutoff* (Å)
H	H	0.076276	2.316	5.396
H	C	0.072074	2.762	6.435
H	R	0.088578	2.940	6.850
H	CH_4	0.149867	3.067	7.146
C	C	0.084067	3.207	7.472
C	R	0.106810	3.385	7.887
C	CH_4.	0.157335	3.512	8.183
R	R	0.138798	3.564	8.304
R	CH_4	0.202163	3.690	8.598
CH_4	CH_4	0.294457	3.817	8.894

*Mixed species parameters for the penetrant–polymer interaction are found with the Lorentz–Berthelot combining rules
†Throughout this work, only a single penetrant is present. The penetrant–penetrant row is included only to show the pure species parameters.

Bonded geometry and interaction parameters:

bond	*l*(Å)	*angle*	k_ϕ(kcal/mol)	*angle*	k_θ(kcal/mol rad^2)	θ_0(deg)
C—C	1.53	C—C—C—C	2.8	aC—C—C	72.2	72.41
C—H	1.10			cC—C—C	72.2	68.0608
C—CH_3	1.53			R—C—C	72.2	68.4738
				R—C—R	72.2	62.2056
				H—C—H	—	73.4205

Torsion angles ϕ_i, defined by Flory's convention of $\phi=0$ in a *trans* conformation [39], contributed

$$\mathcal{V}^{\phi} = \sum_i \frac{1}{2} k_{\phi}(1 - \cos 3\phi_i) \tag{3}$$

to the potential, where all torsion angles had the same constant k_{ϕ}, taken from the work by Suter and Flory [33].

A Lennard-Jones potential

$$\mathcal{V}_{LJ}^{\text{pen}}(r_{ip}) = 4\epsilon_{ip}\left[\left(\frac{\sigma_{ip}}{r_{ip}}\right)^{12} - \left(\frac{\sigma_{ip}}{r_{ip}}\right)^{6}\right] \tag{4}$$

$$\mathcal{V}_{LJ}^{nb}(r_{ij}) = 4\epsilon_{ij}\left[\left(\frac{\sigma_{ij}}{r_{ij}}\right)^{12} - \left(\frac{\sigma_{ij}}{r_{ij}}\right)^{6}\right] \tag{5}$$

described non-bonded interactions between the penetrant p and each atom i of the polymer ($\mathcal{V}^{\text{pen}}$) and between atom pairs (i, j) of the polymer that are separated by three or more bonds or belong to different chains ($\mathcal{V}^{nb}$). The pairwise nonbonded potentials were set to zero at a cutoff distance $r_{ij}/\sigma_{ij}=2.33\equiv R_c$, and a quintic spline was used in the range $1.45 < r_{ij}/\sigma_{ij} < R_c$. This form ensured that the potential energy, the force, and the rate of change of the force with respect to separation were continuous at the junction point and throughout the range $r_{ij}/\sigma_{ij} < R_c$, and all three quantities equaled zero at distances greater than the cutoff distance R_c. The total nonbonded energy equaled the sum of the contributions from all penetrant–polymer atom pairs and polymer–polymer atom pairs, using the appropriate formulas based on the pair separation distances.

Pure and mixed parameters for the nonbonded polymer–polymer interactions were calculated using the Slater-Kirkwood relations [33, 40]. In those relations, the dispersion energy term

$$c_{ij} = \frac{3}{2}\frac{e\hbar}{m_e^{1/2}}\frac{\alpha_i\alpha_j}{(4\pi\epsilon_0)^2}\left(\left(\frac{\alpha_i}{n_{ei}}\right)^{1/2} + \left(\frac{\alpha_j}{n_{ej}}\right)^{1/2}\right)^{-1}$$

is a function of the polarizability α and effective number of electrons n_e, while the small-distance repulsion term

$$a_{ij} = \frac{1}{2} c_{ij}(r_{vdWi} + r_{vdWj})^6$$

is determined by requiring the intermolecular force to equal zero at the sum of the van der Waals radii $r_{vdW_i} + r_{vdW_j}$. Equivalent Lennard-Jones parameters

$$\epsilon_{ij} = \frac{1}{4}\frac{c_{ij}^2}{a_{ij}} \tag{6}$$

$$\sigma_{ij} = \left(\frac{a_{ij}}{c_{ij}}\right)^{1/6} = 2^{-1/6}(r_{vdW_i} + r_{vdW_j}) \tag{7}$$

were used in Eq. (5). Penetrant parameters were taken from Refs [41, 42]. Mixed species parameters for the penetrant/polymer interactions were calculated with the Lorentz-Berthelot combining rules [35].

Initial polymer structures (devoid of any penetrant) were generated according to the method of Theodorou and Suter [34]. Geometric analysis was then used to identify approximate sorption states and diffusion paths for a helium-sized hard sphere probe in the static polymer matrix [43]. We then searched for saddle points on the three-dimensional penetrant–polymer potential energy hypersurface, again keeping the polymer chain positions fixed. A narrow "neck" region along each path, as determined by the geometric analysis, served as an initial guess for the penetrant position. The dimensionality of the saddle-point search was progressively increased by including generalized coordinates associated with polymer atoms near the penetrant. (At this point, the polymer chains are no longer static.) Ultimately, the generalized coordinates associated with all atoms that interacted directly with the penetrant were included. The resulting multidimensional transition state was defined by ca. 350 flexible polymer coordinates (torsion angles, bond angles, etc.) in addition to the penetrant position.

The transition state in this approach is a particular configuration of the polymer + penetrant system, in which the potential energy gradient with respect to each generalized coordinate allowed to vary (hereafter called a "flexible" generalized coordinate) equals zero. The diffusion pathway was defined as a sequence of configurations (a curve in the multidimensional configuration space of the polymer + penetrant system), which passes from one local energy minimum to another through the transition state. Diffusion pathways were constructed starting from each transition state, using Fukui's Intrinsic Reaction Coordinate (IRC) [44]. The first step towards each local minimum was directed along the eigenvector $\mathbf{Q}$ that corresponded to the

negative eigenvalue of

$$H_{qq}\mathbf{Q} = \lambda \mathbf{a}^0 \mathbf{Q} \tag{8}$$

where H_{qq} is the Hessian matrix of second derivatives of the potential energy with respect to the flexible generalized coordinates, and $\mathbf{a}^0$ is the covariant metric tensor in the subset of flexible generalized coordinates, which arises when changing from the generalized coordinate system to the mass-weighted Cartesian coordinate system. Subsequent steps $\mathbf{Q}$ were calculated from

$$\mathbf{a}^0\mathbf{Q} = -\nabla_q \mathcal{V} \tag{9}$$

and were thus directed along the local force vector.

The distance Δs traveled in each infinitesimal step along the IRC was found from

$$(\Delta s)^2 = (\Delta \mathbf{Q})^T \mathbf{a}^0 (\Delta \mathbf{Q}) \tag{10}$$

where $\Delta\mathbf{Q}$ was the change in flexible generalized coordinates along this step; it was parallel to $\mathbf{Q}$ but with a small magnitude. The total distance along the reaction coordinate equals the sum of all (Δs) terms, and it spans the length of the curve followed in multidimensional space by the penetrant–polymer system along the IRC. The zero in s is defined by the location of the transition state. By this definition, the reaction coordinate does not equal the net displacement of the penetrant.

The transition-state theory rate constant is calculated from

$$k^{TST} = \frac{k_B T}{h} \frac{Q^{\ddagger}}{Q} \tag{11}$$

as a ratio of partition functions on the dividing surface and in the local minimum. The partition functions were evaluated by making a harmonic approximation for the potential energy, using the flexible model in the limit of infinite stiffness [37]. In this limit, each partition function can be written as a product of individual vibrational partition functions. Following a suggestion of Gilbert [45], we replace (conceptually) the classical Hamiltonian in the normal-mode coordinates with an equivalent, quantum-mechanical one. This leads to a vibrational partition function

$$q_{\text{vib}\,i}^{QM} = \left[1 - \exp\left(-\frac{h\nu_i}{k_B T}\right)\right]^{-1}$$

for each normal-mode frequency ν_i, calculated from the eigenvalue problem, Eq. (8). Substituting into Eq. (11) leads to the form

$$k^{TST} = \frac{k_B T}{h} \frac{\prod_{\alpha=1}^{f} \left[1 - \exp\left(-\frac{h\nu_\alpha}{k_B T}\right)\right]}{\prod_{\alpha=2}^{f} \left[1 - \exp\left(-\frac{h\nu_\alpha^\ddagger}{k_B T}\right)\right]} \exp\left(-\frac{(\mathcal{V}^\ddagger - \mathcal{V}_0)}{k_B T}\right) \tag{12}$$

where f equals the number of flexible degrees of freedom throughout the jump, ‡ indicates quantities calculated at the transition state, and the exponential arises because the harmonic approximations are made about points with different energies $\mathcal{V}^\ddagger$ and $\mathcal{V}_0$. A preliminary description of the distribution of jump rate constants has appeared previously [46], and a full derivation has been submitted elsewhere [32].

2.1. Macrostates

The geometric analysis in Ref [43] was undertaken on the assumption that regions in a static polymer matrix that are accessible to a hard sphere probe are more likely to be visited by a soft-sphere penetrant in a fluctuating matrix than are regions inaccessible to the probe. However, each cluster of accessible volume is not a single local minimum on the total potential energy hypersurface: the shape of each accessible cluster changes with polymer configuration fluctuations, and, for each configuration sampled, numerous local energy minima exist for the penetrant within each accessible cluster. Each of these local minima may be called a "state", and the accessible cluster could be partitioned into a number of individual states. A fluctuating penetrant–polymer system, such as one observed in a molecular dynamics simulation, would visit these different states according to their Boltzmann-weighted probabilities, since these states are separated by energy barriers that are small relative to the thermal energy $k_B T$. The time required to move from any one state to another would then presumably be small. We term such a collection of penetrant sorption states a "macrostate", since their closely residing local energy minima correspond to different positions for the sorbed penetrant within fairly similar polymer configurations.

Distinct macrostates are those separated by energy barriers much larger than $k_B T$. Passage between them is then an infrequent event, and studying such transitions with transition-state theory is appropriate. The jumps found with the methods outlined above can be divided into two categories:

jumps between states that lie in different macrostates (inter-macrostate), and jumps between states that are within the same macrostate (intra-macrostate). Inter-macrostate jumps are crucial to penetrant diffusion in a glassy polymer, since without them a penetrant would remain trapped in a single sorption macrostate of molecular dimensions. Though it isn't valid to apply a TST-based approach to jumps within a single macrostate (since they cross energy barriers of order k_BT), such results are included here to demonstrate the partitioning of configuration space into macrostates and to provide a basis against which the inter-macrostate jump results may be compared.

3. RESULTS

3.1. Illustrations of Penetrant Jumps

Visualizations of three different methane jumps within glassy atactic polypropylene are shown in Movies 1, 2, and 3. The jumps were obtained using the methods described in the previous section, and each jump was based on a different pure-polymer configuration. The green spheres depict the backbone carbon atoms, the white spheres depict the pendant hydrogen force centers, the red spheres depict the united-atom methyl groups, and the blue sphere represents the jumping methane united-atom molecule. Periodic boundary conditions are in effect, and the thin white lines indicate the "edges" where one copy of the simulation cell is connected to the next. Successive frames are separated by 1.25 Å along the IRC in Movie 1 and by 1.0 Å along the IRC in Movies 2 and 3.

In Movie 1, the cell is situated such that the methane originates near the front center of the cell and jumps towards the inside. The jump is accompanied by three main polymer motions: a backbone chain segment bends slightly to move a side group from the penetrant's eventual path; another segment rotates as its side group follows the methane; and a third chain segment lifts itself above the path, descending after the methane passes. Near the sides of the cell, very little motion is observed. The broad motions of the polymer chains result from coupled, simultaneous changes in many degrees of freedom (bond angles, torsion angles, overall orientation), and the pathway for the penetrant exists because these motions occur together. On-off "flickering" of some spheres results from switching between different periodic images of particular atoms occupying the parent cell.

The path shown (the IRC) is a theoretical construct that tracks the minimum energy path [44], and to follow it exactly would require

continuous quenching of the kinetic energy after each step [47]. The true path followed by a system at a finite temperature, as would be observed in a molecular dynamics simulation, would fluctuate about the IRC, sampling other points that differ in energy by ca. k_BT [48]. The only meaningful time to emerge from this approach, the inverse TST rate constant $1/k^{TST}$, equals the average waiting time before the jump occurs. The time required for the jump to be completed, once it has started, would be much shorter than this waiting time, but cannot be computed within the TST framework.

The simulation cell in Movie 2 is situated such that the methane begins near the top and then jumps down and to the right. During the first half of the jump, little polymer motion occurs, as the methane moves towards the edge of a sorption macrostate. Next, the penetrant appears to slow down, and displacement along the IRC consists mainly of local polymer motions, which begin to widen a channel above and behind the methane. Finally, the methane enters this channel, the polymer chains move back, and the jump is complete. Most polymer motions occur near to the penetrant, and again the atoms far away do not move significantly.

Movie 3 demonstrates a physical picture similar to Movies 1 and 2. The jump begins as three methyl groups separate from one another. After the methane passes through the widened opening, the groups return to their initial positions. Most atoms far from the jump event remain stationary. Flickering is again due to subtle atom motions at the periodic boundary.

A penetrant jump can also be visualized by displaying where polymer chains do not reside. A method for determining where the center of a hard sphere probe can reside without overlapping with the surrounding chains within an instantaneous polymer configuration was developed in Ref [43]. This method essentially invokes (1) drawing a sphere about each atom on the polymer, with a radius equal to the sum of the atom's van der Waals radius and a probe radius, r_p, with $r_p = 1.28$ Å used here; (2) calculating which points (x, y, z) fall outside all of the spheres; and (3) plotting all such points in three dimensions. Points that are connected together are called "clusters of accessible volume", and they correspond to a sorption macrostate.

Shown in Figure 1 are the changes in accessible volume along the multidimensional diffusion path animated in Movie 3. The reactant state, on the left, shows the penetrant (now a red sphere) at the edge of a sorption macrostate. The transition state (center) is formed by the concerted polymer motions that opened a channel for the penetrant, coupled with penetrant translation to a point midway between the reactant and product states. In the product state (right), the penetrant has moved to a different macrostate,

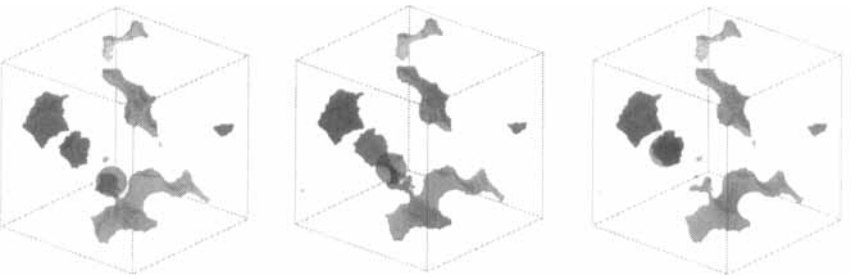

FIGURE 1 Visualization of volume accessible to a helium-sized probe along the IRC for one jump. The center picture, corresponding to the transition state, shows an open channel with the penetrant (red) near its center. The left and right pictures show the reactant and product states, respectively. Though methods from Ref [43] were used, the penetrant and polymer interacted energetically (See Color Plate VI).

corresponding to a different cluster of accessible volume, and the polypropylene chains have closed the channel through which the methane jumped. Though the penetrant has jumped between different macrostates, the polymer shape, as monitored by the volume accessible to a helium-sized probe, has returned close to its initial conformation.

Figure 2 displays the paths followed by carbon and methyl interaction sites during this particular jump. Sites that experienced a maximum displacement of at least 0.33 Å during the jump have their paths shown as thin lines. The penetrant's path is shown as a thick line. A circle indicates the transition state location and an arrow indicates the penetrant position at the end of Movie 3. Displacements of polymer interaction sites were small and were confined to a region very near the penetrant. As implied by Movie 3, a number of these displacement paths are shaped like open loops: an interaction site on the polymer moves away from the penetrant's path to create a channel, the penetrant passes by the displaced atom, and the loop is closed by the return of the displaced atom to its original position. No reciprocating motions were imposed on the system. They arose as a natural consequence of following the IRC along the penetrant–polymer potential energy hypersurface.

Profiles of the potential energy along the reaction coordinate for the jumps in Movies 1–3 are shown in Figure 3. The total energy is shown as a solid line, and its components are indicated by labels and broken lines. Energy and position changes along the IRC were smooth, and no discontinuities in the diffusion path were observed when a sufficient number of generalized coordinates near the penetrant were considered flexible. The different energy components will be discussed below.

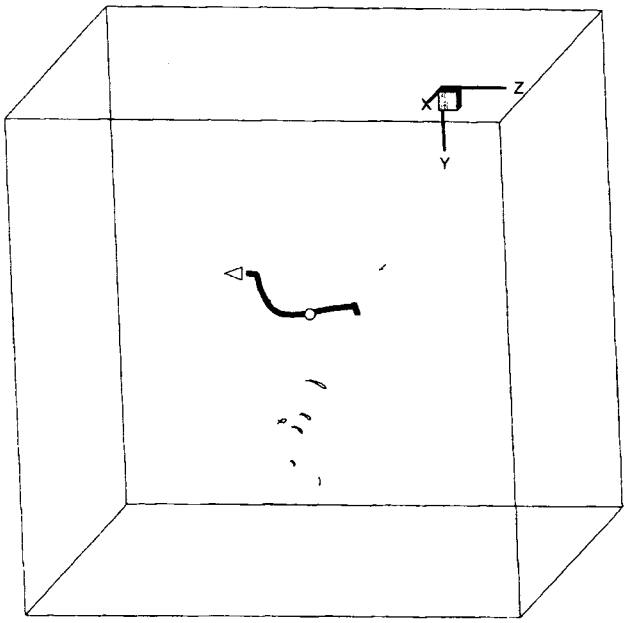

FIGURE 2 Example of heavy atom displacement for one penetrant jump. The heavy line shows the path followed by the penetrant. The thin lines show the paths followed by carbon atoms and methyl groups that moved at least 0.33 Å away from their location at the transition state.

The energy barriers ($\Delta\mathcal{V}=\mathcal{V}^{\dagger}-\mathcal{V}_0$), rate constant ($k^{TST}$), and jump lengths ($\ell$) are listed in Table II. The potential energy barriers for these jump events, in the range of several kcal/mol, are significantly larger than the thermal energy k_BT, equal to 0.46 kcal/mol at 233 K, and thus validate one of the underlying assumptions of TST. Although these energy profiles (and associated jump rates and jump lengths) are typical, not all jumps have exactly those energy profiles, jump rates, etc. The distributions observed in a series of methane-in-polypropylene simulations have been presented elsewhere [31, 32]. Mechanistic aspects, averaged over the same set of jumps, will be discussed in the remaining sections.

3.2. Participation Ratio

Over short time scales, fluctuations of a glassy system around its minimum energy configuration of stable mechanical equilibrium can be treated by a harmonic approximation. Net particle displacements are linear super-

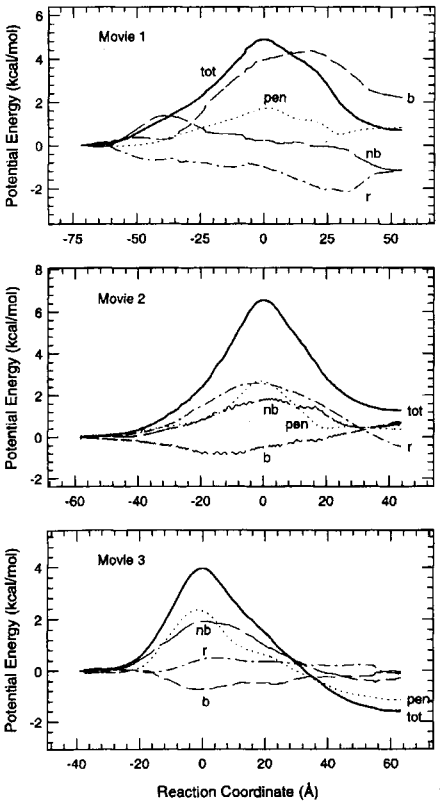

FIGURE 3 Change in energy along the IRC for the jumps visualized in Movies 1–3. The reaction coordinate (abscissa) includes contributions from both penetrant and polymer chain motions.

TABLE II Properties of sample jumps visualized in Movies 1–3. $\Delta\mathcal{V}$ indicates the total energy barrier, k^{TST} indicates the jump rate constant, and ℓ indicates the three-dimensional distance between the penetrant positions at the path endpoints. Subscripts distinguish between quantities in the forward (f) and backward (b) directions

Movie	$\Delta\mathcal{V}_f$ *(kcal/mol)*	$\Delta\mathcal{V}_b$*(kcal/mol)*	$k_f^{TST}(\mu s^{-1})$	$k_b^{TST}(\mu s^{-1})$	$\ell(\text{Å})$
1	4.90	4.17	29.6	63.3	5.32
2	6.56	5.27	5.97×10^{-3}	1.98	5.87
3	3.96	5.54	63.1	0.288	6.39

positions of motions along the normal modes of the system (or eigenvectors of the Hessian matrix of second derivatives of the potential energy with respect to mass-weighted Cartesian coordinates, Eq. (8)). The participation ratio [49] characterizes whether motions along particular normal modes are

local, global, or some combination thereof, through the use of "energy-moments". The velocity of one atom j that can be attributed to a particular mode, denoted by $\mathbf{r}$, may be written as

$$\mathbf{v}_j = 2\pi\nu \begin{pmatrix} X_j \\ Y_j \\ Z_j \end{pmatrix} \sin(2\pi\nu t) \tag{13}$$

where $\mathbf{v}_j$ is the (vector) velocity of atom j, ν is the frequency of the mode, and X_j, Y_j, and Z_j are amplitudes that correspond to the displacement of atom j in this mode along the three Cartesian coordinate axes. m_j will denote the mass of atom j. (Hydrogen atoms will retain their own mass in this analysis.) The total kinetic energy of this particular mode,

$$\begin{aligned} KE &= \frac{1}{2}\sum_j m_j |\mathbf{v}_j|^2 \\ &= 2\pi^2\nu^2 \sin^2(2\pi\nu t) \sum_j m_j \begin{pmatrix} X_j \\ Y_j \\ Z_j \end{pmatrix} \cdot \begin{pmatrix} X_j \\ Y_j \\ Z_j \end{pmatrix} \end{aligned} \tag{14}$$

contains a series of terms,

$$\epsilon_j \equiv m_j(X_j^2 + Y_j^2 + Z_j^2)$$
$$\epsilon_j \equiv (x_j^2 + y_j^2 + z_j^2)$$

one from each atom. The symbols x_i, y_i, z_i correspond to mass-weighted Cartesian coordinates, $x_i = m^{1/2}X_i$. The sum of such terms raised to the power n

$$M_n \equiv \sum_{j=1}^{N\times N_c + N_{\text{pen}}} (\epsilon_j)^n \tag{15}$$

corresponds to the n'th energy moment for this mode. The zeroth moment, M_0, equals the total number of atoms $N_{\text{tot}} = N\times N_c + N_{\text{pen}}$. The first moment, M_1, is proportional to the total energy of the mode. Bell and Dean [49] defined the effective number of atoms participating in a mode α as

$$N_\alpha^{EFF} = \frac{M_1^2}{M_2} \tag{16}$$

where M_2 is the second energy moment. The participation ratio is defined by

the ratio of $N_\alpha{}^{EFF}$ to the zeroth moment M_0

$$p = \frac{M_1^2}{M_0 M_2}$$

and it approximately equals the fraction of atoms that are displaced when a particular mode is activated.

For determining penetrant jump rates with the penetrant–polymer system considered here, the normal modes at the local minima and the transition state were calculated in the local flexible generalized coordinates $\mathbf{q}$. To calculate the effective number of participating atoms, it is necessary to convert each mode from generalized to mass-weighted Cartesian coordinates. To do so, we expand the elements of Eq. (16) in terms of their x, y and z mass-weighted coordinates,

$$N_\alpha^{EFF} = \frac{\left[\sum_{\text{atoms } j}\left((x_j^\alpha)^2 + (y_j^\alpha)^2 + (z_j^\alpha)^2\right)\right]^2}{\sum_{\text{atoms } j}\left((x_j^\alpha)^2 + (y_j^\alpha)^2 + (z_j^\alpha)^2\right)^2} \tag{17}$$

(α distinguishes the particular mode) and substitute for each contribution by converting to flexible generalized coordinates,

$$(x_j^\alpha)^2 = \left(\sum_{k=1}^{f} \frac{\partial x_j}{\partial q_k} Q_k^\alpha\right)^2$$

$\mathbf{Q}^\alpha$ denotes the eigenvector with respect to the local flexible generalized coordinates. For a mode in which a single atom moves, only that atom contributes to the sums in the numerator and denominator, yielding a ratio of unity. For a mode in which the penetrant and all atoms on all chains contribute equally, each atom's contribution is approximately $1/N_{\text{tot}}$. The numerator of Eq. (17) is a sum of N_{tot} such terms, yielding $(N_{\text{tot}} \times 1/N_{\text{tot}})^2 = 1$. Each term in the lower sum equals approximately $1/(N_{\text{tot}})^2$, so the sum of N_{tot} terms is about $1/N_{\text{tot}}$, yielding an effective number of atoms equal to N_{tot}. For modes involving only N atoms, such as overall translation or rotation of a single chain, the same calculations yield an effective number of participating atoms equal to N. For modes that are intermediate in size between a single atom and a single chain, the effective number of participating atoms will vary between these limits.

The averaged effective number of participating atoms is shown in Figure 4 as a function of the frequency ν of the mode. Following the practice used in the Instantaneous Normal Mode analysis of liquids [50], the results for modes with imaginary frequencies ν, of which there is one per penetrant jump, are shown at the position $i\nu$ on the negative frequency axis. These imaginary frequencies can only be contributed by the single negative eigenvalue found at a saddle point. Otherwise, the results for the minima and transition states are essentially identical. The lowest frequency modes ($\nu < 12\,\text{cm}^{-1}$) involve coupled motions of a few chains (see the related discussion in the "Changes in Generalized Coordinates Along the IRC" section), while the remaining modes with frequencies below $100\,\text{cm}^{-1}$ involve fewer atoms than those comprising a single chain. A slight difference between the minima and transition states exists at 14 cm^{-1} (see inset), where the modes found at local minima tend to involve of order ten fewer atoms than do the modes of the same frequency at the transition states. This difference, though small, persisted among the different possible resolutions available for tabulating the simulation data. The modes with imaginary frequencies tended to involve only one atom, the jumping penetrant, as seen by the low value of N_{EFF}. These results are similar to those presented recently for atactic polypropylene containing a single tetrazine molecule [51] in the region from 15–200 cm^{-1}, even though a different potential representation was used there. The high participation seen here along modes of extremely low frequency, which we attribute to shuttling motions of an entire chain, could not have been observed in Ref [51], since the molecular structures used there contained only a single chain. Forrest *et al.* observed a peak between 200 and 400 cm^{-1}, which they attributed to mixing between tetrazine and polypropylene modes; the lack of such a peak here adds further support to their arguments. Even higher participation ratios of $p \approx 0.55$, which signify more extended modes, were found with similar calculations on monatomic glasses [52].

The relative number of normal modes as a function of frequency is shown in Figure 5. By comparing with Figure 4, it is seen that most normal modes are of low frequency and involve a significant number of atoms, though very few involve shuttling motions of multiple chains. While the distribution again agrees favorably with the simulation results of Forrest *et al.* [51], the relative distribution of frequencies seen here does not resemble the experimental far-infrared absorption spectrum of polypropylene [53]. This is not too surprising, since bond lengths, which strongly affect the infrared spectrum, have been considered infinitely stiff throughout these simulations. In addition, no effort has been made to restrict Figure 5 to modes that

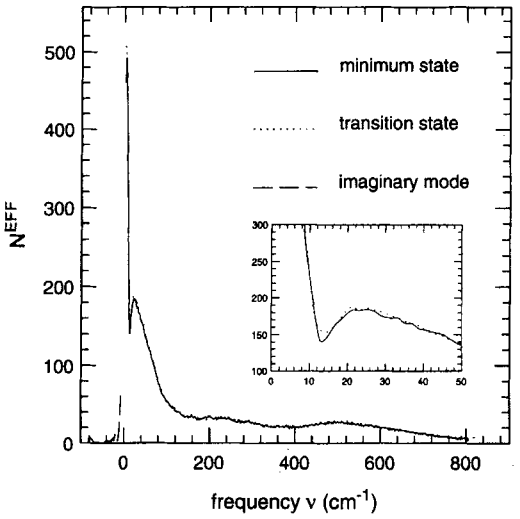

FIGURE 4 Effective number of participating atoms as a function of harmonic frequency. Modes with imaginary frequencies are shown at *iv* on the negative frequency axis; only one such mode existed per jump. The inset exaggerates the region near 14 cm^{-1}, where a slight difference in N^{EFF} exists between minima and transition states. The participation ratio is obtained as $p = N^{EFF}/N_{tot}$ where $N_{tot} = 898$ (total number of atoms) for all cases.

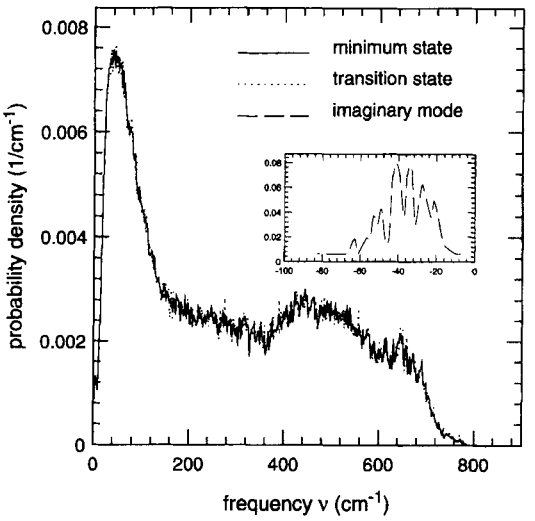

FIGURE 5 Average distribution of harmonic frequencies at the local minima and transition states. The main plot shows the distribution of real frequencies; the inset shows the same information for imaginary frequencies at the postion *iv*. One cannot identify a single frequency that becomes imaginary at the transition state; that frequency varies from jump to jump.

would be spectroscopically active. In general, far more normal modes exist than would be spectroscopically allowed by selection rules [54].

3.3. Displacement of Heavy Atoms During a Penetrant Jump

Movies 1–3 showed clearly that conformation changes along the IRC have a concerted effect – carbon and methyl interaction sites on the polymer chains are displaced away from the path followed by the penetrant. The size of the local region over which atoms of the polymer are displaced during a penetrant jump motion is quantified in this section by calculating the distance that atoms of the polymer move as a function of their distance from the penetrant position at the multidimensional transition state. First, the locations of all carbon atoms and methyl groups (all heavy atoms) at the multidimensional transition state were noted. Next, the reaction coordinate was traversed in the forward and reverse directions, and the magnitude of each atom's displacement from its transition state location was recorded throughout.

Plotted in Figure 6 is the maximum displacement observed anywhere along the reaction coordinate for heavy atoms, as a function of their distance from the penetrant location when in the transition state configuration. The two sets of curves were averaged over all inter- or intra-macrostate jumps simulated. The first observation for the inter-macrostate jumps is that atoms at all distances from the penetrant exhibited an average displacement of ca. 0.1 Å. This important point will be discussed in the "Changes... Along the IRC" section. The region in which the displacement is significantly larger than this baseline level extends about 9Å away from the transition state location. For comparison, the maximum distance used in generating the list of flexible degrees of freedom in the construction of the diffusion path equaled

$$(2.33 + 0.2) \times \frac{1}{2}(\sigma_{RR} + \sigma_{pp}) = 10.5 \text{ Å}$$

suggesting that enough generalized coordinates were considered flexible, since some atoms capable of changing their position remained in place relative to more distant atoms. (Atoms far from the jump event didn't move during the animations.) The largest displacement near the transition state location of the penetrant were those of methyl groups, shown by the top curve, while backbone carbon atoms on achiral segments moved the least. The displacement averaged over all heavy atom types is nearest to that of

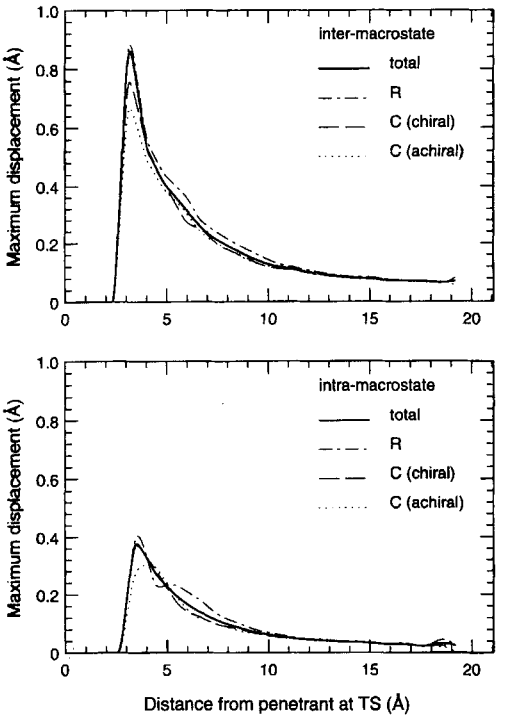

FIGURE 6 Maximum displacement of heavy atoms along the IRC, plotted against the distance between the heavy atom and the penetrant while the system is in the transition state configuration. Separate plots are shown for inter- and intra-macrostate jumps. For the inter-macrostate plot (starting from the top), the four curves are averaged over all pendant methyl groups, all heavy atoms, all backbone atoms on chiral segments, and all backbone atoms on achiral segments. The curve for all heavy atoms is near that of the pendant group for small distances, since few backbone carbon atoms are that close to the penetrant. Displacement curves are similarly labelled for intramacrostate transitions.

the methyl groups since there are more methyl groups near to the penetrant than there are backbone carbon atoms.

This result, if valid for other polymers with pendant groups, could suggest a more precise definition of the mechanisms invoked in phenomenological models to explain existing diffusion data. The role of chain stiffness may not be merely to control bending of chain backbones in order to create a hole, as used in the Brandt [2] and Pace–Datyner [3–5] models. If a backbone merely had to move out of the way, the displacement of all atom types should be similar. The simulations presented here show that the pendant groups in polypropylene near to the penetrant move significantly further. This suggests that "chain bending" must also include simultaneous chain

twisting, the difficulty of which would depend on the torsion angle and its proximity to a *trans* or *gauche* state. Another interpretation is that the effect of increasing chain stiffness is really to increase the difficulty with which pendant groups may be moved out of the way; this would make enlarging a channel through which the penetrant may pass more difficult.

The heavy atom displacement during jumps that remained within a macrostate was much smaller. The heavy atoms near the penetrant moved by 0.4 Å or so, while distant atoms shifted by less than 0.03 Å. The energy barriers for these jumps were small because significant polymer motions were not required to create an open diffusion channel.

3.4. Energy Profiles

Although the total potential energy along each diffusion pathway exhibited a peak at the transition state, the relative contributions from each energy type (penetrant–polymer, polymer–polymer, bond angle bending, torsion angle rotation) differed from jump to jump. In some cases, different energy components would remain constant, exhibit peaks elsewhere, or even exhibit multiple peaks along the diffusion path. The total potential energy still decreased monotonically as the penetrant passed from the transition state to the corresponding local minima; along some steps a significant decrease in one energy type would be counter-balanced by increases in another.

All inter- and intra-macrostate jumps were grouped into different categories, depending on how much each energy component changed relative to the others and to the total potential energy barrier. The different categories are listed in Table III, along with their relative percentage of occurrences and average jump rate constants. Significant differences in jump types are clear between inter- and intra-macrostate jumps. Just under half of the inter-macrostate jumps involved changes in all four energy types, with the bending and torsional contributions being opposite to one another in a third of those cases.

The jumps animated in Movies 1 and 2 involved changes in all four energy types, as can be seen in Figures 3a and 3b. The jump animated in Movie 3 falls in the "pen,nb" category, as seen in Figure 3c. Despite the visual similarities of the three movies, the underlying energy profiles are very different, especially for the energy components. The need to include changes in polymer degrees of freedom can be seen in the magnitudes of the energy components. If the penetrant were simply "smashing through" a hole, the penetrant–polymer energy would rise, while the other components would remain constant. Instead, many different components change, with some

TABLE III Types of penetrant jumps, based on potential energy changes along the IRC. The percentage indicates the number of inter- and intra-macrostate jumps of each type relative to the total number of jumps simulated. The rate constants listed are the geometric means over all inter- or intra-macrostate jumps within a particular category

*Changing components**	*%(inter-)*	$\overline{k^{TST}}(\mu s^{-1})$	*%(intra-)*	$\overline{k^{TST}}(\mu s^{-1})$
pen (mainly)	4.3	1610.	24.4	235000
nb (mainly)	5.5	8.94×10^{-4}	0	–
bend	0	–	2.2	52050
pen, nb	11.7	0.421	4.4	240400
pen, rot	0	–	4.4	305000
pen, bend	1.8	1.58	4.4	23400
nb, rot	1.2	1785.	0	–
nb, bend	0.6	1.90	2.2	605
pen, nb, (rot, bend)†	12.3	7.79	4.4	65700
pen, nb, rot	9.2	0.114	6.7	133600
pen, nb, bend	11.7	0.260	4.4	1450
pen, rot, bend	0.6	542.	4.4	1140
nb, rot, bend	5.5	82.9	20.0	2880
pen, nb, rot, bend	35.6	0.732	17.8	1000

*Components are labeled and defined as follows:

pen penetrant–polymer nonbonded energy (Lennard-Jones)

nb polymer–polymer nonbonded energy (Lennard-Jones)

rot torsional energy (sinusoidal in 3ϕ)

bend bond angle bending energy (harmonic in θ)

†Jumps in which the torsional and bending energy changes counter-balance (are equal and opposite to) one another at each point along the IRC

interactions even becoming *more* favorable during a jump, such as the torsional energy in Figure 3a.

Comparing the average inter-macrostate rate constants for each jump type, three ranges are seen. Jumps over barriers in mainly the penetrant-polymer energy are very fast; their average rate constant of 1610 $\mu s^{-1} = 1.61\ ns^{-1}$ suggests that these jumps could be observed in long molecular dynamics simulations. Jumps over barriers in penetrant–polymer energy and some combination of polymer–polymer, bending, and torsional energy comprise the largest group. Their average rate constants tend to be of order $0.1 - 10\mu s^{-1}$. These jump types are important for penetrant diffusion because they are so numerous; faster jumps, taken alone, do not encompass enough of the total jump population to enable formation of connected paths across macroscopic distances. (The fraction of faster jumps is below the bond percolation threshold for the network of sites occupied by the penetrant.) The slowest jumps involve mainly changes in the polymer–polymer nonbonded energy.

Jumps within macrostates tended to involve fewer types of energy changes. Those involving mainly changes in penetrant–polymer energy

were very fast, while jumps involving changes in three or four energy types were slower, and approached the rate constants of the fastest inter-macrostate jumps. These similarities blur to some extent the grouping of local minima (sites) into macrostates and the distinction between inter-macrostate and intra-macrostate jumps. However, the distinction is still meaningful, since the majority of inter- and intra-macrostate jumps have rates significantly slower or faster, respectively, than jumps in this crossover region.

3.5. Changes in Generalized Coordinates Along the IRC

Along the IRC, the values of the chain start positions and of the various bond, torsion, and Eulerian angles that define the polymer configuration change, while the penetrant jumps between sites. A reasonable question to ask is whether a correlation exists between the size of the change in the generalized coordinates and the jump rate constant. This question was investigated by calculating for each jump the maximum change (regardless of sign) in any angle and in any chain-start position along the IRC. In most cases, the angle changing by the most was a torsion angle; in the few remaining cases an Eulerian angle changed by more. There were no cases in which the change in a bond angle was larger than any of the ten largest torsion and Eulerian angle changes. In many cases, two of the three largest changes were along torsion angles or Eulerian angles near each other on a single chain. This suggests a coupling of two or more angles along the IRC. No such coupling was included explicitly in the potential energy; it must have arisen indirectly through the penetrant–polymer or polymer–polymer nonbonded interactions.

A scatter plot of the jump rate constant and maximum torsional change along the IRC is shown in Figure 7. No simple functional form is evident for relating these two quantities. Some slight correlations do exist: extremely slow jumps tend to have large changes in at least one torsion angle, and few fast jumps exhibit large changes in any torsion angle. For jumps in which the maximum change in a torsion angle was small, the slowest jump rate varied from 10 μs^{-1} at 5° to 10^{-6} μs^{-1} at 20°, while the fastest jumps remained on order $10^6 \mu s^{-1}$. However, this range of rate constants encompasses the majority of probable jump rates, according to the distribution we report in Refs [31, 32].

Examining the maximum change in chain start positions along the IRC revealed a disturbing trend. In almost all jumps, a chain start would shift its position on the order of tenths of Ångstroms. For a single atom, this would

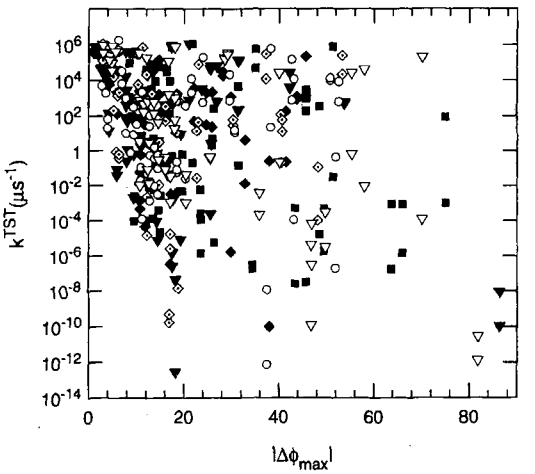

FIGURE 7 Scatter plot of the jump rate constants and associated maximum torsion angle change along the IRC. Different symbols indicate jumps based on different initial polymer structures.

mean nothing; however, all atom positions depend explicitly on the chain start position. These slight shifts, which are signified in Figure 4 by a large number of atoms participating in a low-frequency mode, cause a third of the atoms in the periodic simulation cell to shift in unison. This effect is evident in Figure 6 as well, which shows that atoms far from the penetrant's transition state position shift on average by 0.1 Å during inter-macrostate jumps.

This uniform shift in chain position is a weakness in the approach we have pursued. Translation of the entire system was prevented by constraining the chain start position for the first chain. However, effective motions of the first chain start manifested themselves as concerted overall motions of the other two chains. This ineffective method for moving the first chain start in cases when it neighbored the penetrant suggests that, in future work, a better method should be chosen for constraining translation of the system as a whole. (One possible method would involve constraining the chain start furthest from the penetrant. Another would involve constraining the center of mass of the three parent chains.) In some ways, chain shuttling is an artifact of periodic boundary conditions, since the interactions between a part of one chain and different parts of its periodic images do not depend at all on the chain start position. In a similar vein, the shift suggests that the simulation cell used was too small. In a larger cell, a chain of the same size would interact with fewer of its images, since a larger number of chains

would be present, and translational modes of the entire chain would be more quenched. Longer chains would probably quench these block motions too, since any particular chain would become more entangled as its length increased. A larger simulation cell would still be required, though, in order to prevent uniform shifting of large parts of the entire cell.

3.6. Chain Start Influence

It is generally accepted that chain ends increase the rate of local relaxations in polymeric solids [55]. If so, then the penetrant jump rate constant near a chain end should be enhanced relative to its average value. To investigate this effect, we determined the distance to the nearest chain start or end from each transition state location of the penetrant. This distance and the associated forward and backward jump rate constants were added to a data set. Using this set, we calculated the geometric mean of all jump rate constants found within a specified distance (d, $d+\Delta$) from a transition state.

The results are plotted in Figure 8. The rate constants for jumps within ca. 5 Å of a chain start or end are an order of magnitude faster (on average) than are jumps that are further away from a chain start or end. A scatter plot of the jump rates as a function of the distance to the nearest chain start or end (shown in Fig. 9) indicates that the increase in the average is due to a lack of slow penetrant jumps, rather than to an increase in the rates of the fastest jumps. This suggests that enhanced diffusion due to chain ends is limited to distances comparable to a few bond lengths (or to the size of a sorption macrostate). It further suggests that the slowest jumps in the rate constant distribution are due to mechanisms not possible near a chain start or end, such as coupled motions of polymer segments that are constrained by their connectivity.

The chain start density in our system,

$$\frac{\rho}{M_n} = \frac{6 \text{ starts and ends}}{(22.791194\text{Å})^3}\left(\frac{10^8\text{Å}}{\text{cm}}\right)^3\left(\frac{1 \text{ mol}}{6.0221 \times 10^{23}}\right) = 8.42 \times 10^{-4} \text{ mol/cm}^3$$

is a factor of 10–100 higher than in commercial samples of polypropylene, due to the small chain length used. 23% of the penetrant jumps simulated were near (within 5 Å) of a chain end, suggesting that the jump rate constants calculated here may be somewhat larger than those in glassy atactic polypropylene of higher molecular weight. The population of jumps

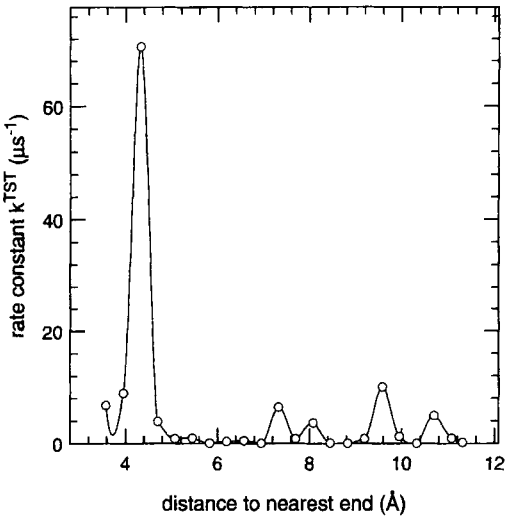

FIGURE 8 Dependence of the jump rate constant on chain end proximity. The x-axis indicates the distance to the nearest chain start or end when the penetrant–polymer system resides in the transition-state configuration.

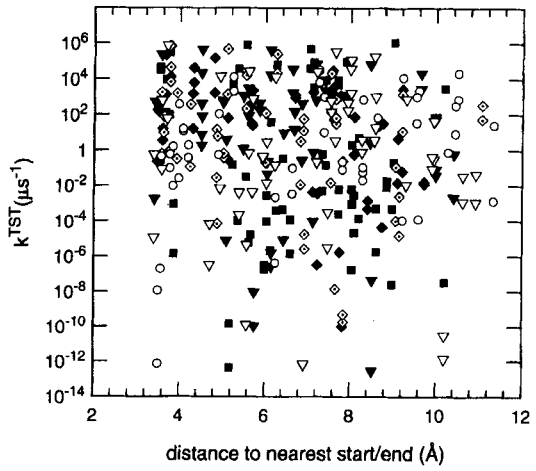

FIGURE 9 Scatter plot of the jump rate constant as a function of chain start/end proximity. The x-axis indicates the distance to the nearest chain start or end, as in Figure 8. Each symbol indicates a different combination of jump rate and nearest chain start distance.

that correspond to the large-distance region of Figure 8 would increase in a sample of higher molecular weight, and hence the distribution of jump rate constants would be shifted towards slower jumps.

4. DISCUSSION

The magnitude of the polymer atom displacement during methane jumps, 0.1 – 1.0 Å, is somewhat larger than the smearing parameter $\langle\Delta^2\rangle^{1/2} = 0.46$ Å reported by Gusev and Suter [28] for O_2 and N_2 diffusion in polyisobutylene at 300 K. This parameter corresponded to the root-mean-squared displacement of polymer atoms due to elastic motions over a single picosecond. An equivalent parameter for methane in glassy atactic polypropylene would probably be smaller than 0.46 Å, since the parameter $\langle\Delta^2\rangle^{1/2}$ is proportional to the absolute temperature [21]. One might expect the required displacement to be smaller for a jump mechanism that included explicit coupling, reasoning that random displacement fluctuations would require larger amplitudes in order to open sufficiently large holes. However, since the magnitude of atom displacement falls off quickly (with respect to distance from the penetrant) in the calculations here, the region of atom displacements is much more focused than that in the calculations of Gusev and Suter. The technique implemented here also incorporates different-sized fluctuations for different atom types, a method that had been suggested for the $\langle\Delta^2\rangle$-based approach [26] but was not incorporated in Refs [27, 28]. Though both our method and Gusev and Suter's method uses transition-state theory to simulate penetrant diffusion, the underlying details are very different.

There has been some debate in the literature about the changes in polymer conformation that accompany penetrant jump motions. Takeuchi [23] observed conformational transitions at times that were near to but not coincidental with the time of an oxygen jump motion in polyethylene. Pant and Boyd [56] observed a significant decrease in the diffusivity of methane in polyethylene at 400 K when they increased the barrier to torsional isomerization by 50%. However, for polyethylene this temperature falls in the melt regime, in which penetrant diffusion is largely due to the rearrangement of polymer structure, rather than to jumps between pre-existing voids [56]. Stouch and co-workers [57] observed torsional isomerization in conjunction with a diffusive jump of benzene through a hydrated biological membrane at temperatures above the glass transition. In later work [58], they found that a jump motion was not always associated with an instantaneous increase in penetrant kinetic energy. The investigation presented here of generalized coordinate changes along the IRC sheds some light on the situation. At a temperature below the glass transition, most jumps showed torsion angle changes smaller than would be required for a conformational transition, and their associated jump rates spanned the

entire breadth of the jump rate constant distribution. The slowest jumps were distributed fairly evenly among jumps with varying maximum changes in torsion angles.

5. CONCLUSIONS

Multidimensional transition-state theory-based methods for calculating penetrant jump rates were applied to methane diffusion in glassy atactic polypropylene at 233 K. Transition states in penetrant and polymer degrees of freedom were found using the necks of geometrically accessible channels as initial guesses; typically of order 350 degrees of freedom were required to specify the transition state configuration in a manner such that the remainder of the polymer conformation remained undisturbed. Starting from the transition states located in this way, entire transition paths in the multidimensional space of the penetrant + polymer degrees of freedom were determined using Fukui's Intrinsic Reaction Coordinate (IRC) approach [44]. Penetrant jumps were distinguished into inter-macrostate, *i.e.* occurring between clusters of accessible volume, as determined by a geometric analysis of the connectivity of empty spaces in the model polymer [43], and intra-macrostate, i.e. occurring within accessible volume clusters.

Animations vividly demonstrated the changes that occur as a penetrant jumps between macrostates. Coupled polymer chain motions combine to open a channel, which closes again after the penetrant passes through it. The volume accessible, monitored during the jump by a hard-sphere probe, also showed a channel opening.

The participation ratios and harmonic frequencies for normal modes at the local minima and at transition states did not differ significantly from one another. Shuttling motions of multiple chains, which are artifacts of the method of choosing flexible degrees of freedom (and of small chain length and model system size) were evident at frequencies under 10 cm^{-1}. Other modes at frequencies below 200 cm^{-1} involved up to ca. 180 atoms, fewer than on an entire chain, while modes at higher frequencies involved forty or fewer atoms. The imaginary mode (that with a negative eigenvalue) at most transition states involved only one atom, the jumping penetrant; accompanying polymer motions were along directions in which the potential energy increased.

Calculations of the maximum displacement of backbone and pendant atoms of the polymer chains along the IRC quantified the magnitude of chain shuttling vibrations. On average, each atom shifted by ca. 0.1 Å during

each inter-macrostate penetrant jump simulation. Displacements of larger magnitude occurred within 9 Å of the penetrant's transition state location. The largest average displacement was for methyl groups 4 Å away from the penetrant. Backbone carbon atoms exhibited smaller displacements, as on average they were further from the penetrant. These results, if applicable to other penetrant–polymer systems, clarify the meaning of chain stiffness in phenomenological theories of diffusion: stiffness describes the ease with which polymer chains can twist, allowing pendant groups to open a channel for a jumping penetrant.

Energy profiles along the IRC were classified according to how different components of the total energy varied. Noticeable changes in penetrant–polymer nonbonded energy, polymer–polymer nonbonded energy, torsional energy, and bond angle bending energy occurred in a third of all jumps between sorption macrostates, with a mean jump rate constant near the average value.

The jump rate did not correlate simply with changes along particular types of degrees of freedom. Bond angles changed much less than did torsion angles along the IRC. Along most jumps, the maximum torsional change was less than 40°, though along some (mostly slow) jumps, changes of up to 90° were observed.

The mean jump rate constant was higher on average (by an order of magnitude) when the penetrant transition state location was within 5 Å of a chain start or end position. A quarter of the jumps simulated here satisfied that criterion. The chain start/end concentration was high relative to what is expected in high molecular-weight glassy atactic polypropylene, suggesting that the collection of jumps studied may contain a systematically high number of faster jumps.

The wealth of information calculated here confirmed that an infrequent jump picture remains relevant for describing the moderate time-scale behavior of a small gas molecule(methane) in a glassy amorphous polymer (atactic polypropylene). Polymer chain segments contributed significantly to penetrant dynamics over molecular length scales, and their exclusion would have changed the qualitative description of the jump motions irrevocably.

Acknowledgement

We thank Professor Robert Gilbert and Richard Henchman for very stimulating conversations during their visits to Berkeley and Patras in the summer and fall of 1995.

References

[1] Petropoulos, J. H. (1990). Some fundamental approaches to membrane gas permeability and permselectivity, *J. Membr. Sci.*, **53**, 229.

[2] Brandt, W. W. (1959). Model calculation of the temperature dependence of small molecule diffusion in high polymers, *J. Phys. Chem.*, **63**, 1080.

[3] Pace, R. J. and Datyner, A. (1979). Statistical mechanical model for diffusion of simple penetrants in polymers. I. Theory, *J. Polym. Sci. Polym. Phys. Ed.*, **17**, 437.

[4] Pace, R. J. and Datyner, A. (1979). Statistical mechanical model for diffusion of simple penetrants in polymers. II. Applications – nonvinyl polymers, *J. Polym. Sci. Polym. Phys. Ed.*, **17**, 453.

[5] Pace, R. J. and Datyner, A. (1979). Statistical mechanical model for diffusion of simple penetrants in polymers. III. Applications – vinyl and related polymers, *J. Polym. Sci. Polym. Phys. Ed.*, **17**, 465.

[6] Vrentas, J. S. and Duda, J. L. (1977). Diffusion in polymer-solvent systems. I. Reexamination of the free-volume theory, *J. Polym. Sci. Polym. Phys. Ed.*, **15**, 403.

[7] Vrentas, J. S. and Duda, J. L. (1977). Diffusion in polymer-solvent systems. II. Predictive theory for the dependence of diffusion coefficients on temperature, concentration, and molecular weight, *J. Polym. Sci. Polym. Phys. Ed.*, **15**, 417.

[8] Vrentas, J. S. and Duda, J. L. (1977). Diffusion in polymer-solvent systems. III. Construction of Deborah number diagrams, *J. Polym. Sci. Polym. Phys. Ed.*, **15**, 441.

[9] Zielinski, J. M. and Duda, J. L. (1992). Predicting polymer solvent diffusion coefficients using free-volume theory, *AIChE J.*, **38**, 405.

[10] Vieth, W. R. and Sladek, K. J. (1965). A model for diffusion in a glassy polymer, *J. Coll. Sci.*, **20**, 1014.

[11] Paul, D. R. and Koros, W. J. (1976). Effect of partially immobilizing sorption on permeability and the diffusion time lag, *J. Polym. Sci. Polym. Phys. Ed.*, **14**, 675.

[12] Petropoulos, J. H. (1970). Quantitative analysis of gaseous diffusion in glassy polymers, *J. Polym. Sci. Part A-2*, **8**, 1797.

[13] Frederickson, G. H. and Helfand, E. (1985). Dual-mode transport of penetrants in glassy polymers, *Macromolecules*, **18**, 2201.

[14] Barrer, R. M., Barrie, J. A. and Slater, J. (1958). Sorption and diffusion in ethyl cellulose, Part III. Comparison between ethyl cellulose and rubber, *J. Polym. Sci.*, **27**, 177.

[15] Michaels, A. S., Vieth, W. R. and Barrie, J. A. (1963). Solution of gases in polyethylene terephthalate, *J. Appl. Phys.*, **34**, 1.

[16] Sefcik, M. D. and Schaefer, J. (1983). Solid-state ^{13}NMR evidence for gas-polymer interactions in the carbon dioxide-poly(vinyl chloride) system, *J. Polym. Sci. Polym. Phys. Ed.*, **21**, 1055.

[17] Smith, P. B. and Moll, D. J. (1990). ^{2}H NMR investigation of the plasticization effects induced by high-pressure carbon dioxide gas on the molecular dynamics of polymers, *Macromolecules*, **23**, 3250.

[18] Cain, E. J., Wen, W.-Y., Jost, R. D., Liu, X., Dong, Z. P., Jones, A. A. and Inglefield, P. T. (1990). Nuclear spin relaxation mechanisms and mobility of gases in polymers, *J. Phys. Chem.*, **94**, 2128.

[19] Cain, E. J., Wen, W.-Y., Jones, A. A., Inglefield, P. T., Cauley, B. J. and Bendler, J. T. (1991). A dual-mode interpretation of spin relaxation for $^{13}CO_2$ sorbed in polycarbonate, *J. Polym. Sci. Polym. Phys. Ed.*, **29**, 1009.

[20] Stern, S. A., Zhou, S., Araux-Lara, J. L. and Ware, B. R. (1989). Evidence of dual-mode diffusion of small molecules in glassy poly (1-trimethylsilyl-1-propyne) from fluorescence photobleaching recovery, *J. Polym. Sci. C, Polym. Lett.*, **27**, 427.

[21] Gusev, A. A., Müller-Plathe, F., van Gunsteren, W. F. and Suter, U. W. (1994). Dynamics of small molecules in bulk polymers, *Adv. Polym. Sci.*, **116**, 207.

[22] Theodorou, D. N. (1996). Molecular simulations of sorption and diffusion in amorphous polymers, in P. Neogi, editor, *Diffusion in Polymers*, pages 67–142, New York: Marcel Dekker.

[23] Takeuchi, H. (1990). A jump motion of small molecules in glassy polymers: A molecular dynamics simulation, *J. Chem. Phys.*, **93**, 2062.

[24] Sok, R. M., Berendsen, H. J. C. and van Gunsteren, W. F. (1992). Molecular dynamics simulation of the transport of small molecules across a polymer membrane, *J. Chem. Phys.*, **96**, 4699.
[25] Müller-Plathe, F., Laaksonen, L. and van Gunsteren, W. F. (1993). Cooperative effects in the transport of small molecules through an amorphous polymer matrix, *J. Mol. Graphics*, **11**, 118.
[26] Arizzi, S. (1990). *Diffusion of Small Molecules in Polymeric Glasses: A Modelling Approach*, PhD thesis, MIT.
[27] Gusev, A. A., Arizzi, S., Suter, U. W. and Moll, D. J. (1993). Dynamics of light gases in rigid matrices of dense polymers, *J. Chem. Phys.*, **99**, 2221.
[28] Gusev, A. A. and Suter, U. W. (1993). Dynamics of small molecules in dense polymers subject to thermal motion, *J. Chem. Phys.*, **99**, 2228.
[29] Gusev, A. A., Suter, U. W. and Moll, D. J. (1995). Relationship between helium transport and molecular motions in a glassy polycarbonate, *Macromolecules*, **28**, 2582.
[30] Greenfield, M. L. and Theodorou, D. N. (1994). Description of small penetrant jump motions in a polymer glass using transition-state theory, *Polymeric Materials Science and Engineering (American Chemical Society)*, **71**, 407.
[31] Greenfield, M. L. (1996). *Molecular Modeling of Dilute Penetrant Gas Diffusion in a Glassy Polymer using Multidimensional Transition-State Theory*, PhD thesis, University of California, Berkeley.
[32] Greenfield, M. L. and Theodorou, D. N. (1997). *in preparation for Macromolecules.*
[33] Suter, U. W. and Flory, P. J. (1976). Conformational energy and configurational statistics of polypropylene, *Macromolecules*, **8**, 765.
[34] Theodorou, D. N. and Suter, U. W. (1985). Detailed molecular structure of a vinyl polymer glass, *Macromolecules*, **18**, 1467.
[35] Allen, M. P. and Tildesley, D. J. (1987). *Computer Simulation of Liquids.* Oxford University Press.
[36] Mansfield, K. F. and Theodorou, D. N. (1991). Molecular dynamics simulation of a glassy polymer surface, *Macromolecules*, **24**, 6283.
[37] Gō, N. and Scheraga, H. A. (1976). On the use of classical statistical mechanics in the treatment of polymer chain conformation, *Macromolecules*, **9**, 535.
[38] Sylvester, M. F., Yip, S. and Argon, A. S. (1991). Investigation by atomistic simulation of structural differences in the glassy and liquid states of atactic poly(propylene), in R. J. Roe, editor, *Computer Simulation of Polymers*, Pages 105–121: Prentice Hall: Englewood Cliffs, NJ.
[39] Flory, P. J. (1969). *Statistical Mechanics of Chain Molecules*, New York: Wiley.
[40] Pitzer, K. S. (1959). Inter- and intramolecular forces and molecular polarizability, *Adv. Chem. Phys.*, **2**, 59.
[41] Müller-Plathe, F. (1992). Molecular dynamics simulation of gas transport in amorphous polypropylene, *J. Chem. Phys.*, **96**, 3200.
[42] Hansen, J. P. and McDonald, I. R. (1976). *Theory of Simple Liquids*, New York: Academic Press.
[43] Greenfield, M. L. and Theodorou, D. N. (1993). Geometric analysis of diffusion pathways in glassy and melt atactic polypropylene, *Macromolecules*, **26**, 5461.
[44] Fukui, K. (1981). The path of chemical reactions – the IRC approach, *Acc. Chem. Res.*, **14**, 363.
[45] Gilbert, R. G. (1995). Personal communication.
[46] Greenfield, M. L. and Theodorou, D. N. (1995). Distribution of jump rate constants underlying methane diffusion in glassy atactic polypropylene as calculated with transition-state theory, *Polym. Prepr. (Am. Chem. Soc., Div. Polym. Chem.,)* **36**, 687.
[47] Sevick, E. M., Bell, A. T. and Theodorou, D. N. (1993). A chain of states method for investigating infrequent event processes occurring in multistate, multidimensional systems, *J. Chem. Phys.*, **98**, 3196.
[48] Miller, W. H., Handy, N. C. and Adams, J. E. (1980). Reaction path Hamiltonian for polyatomic molecules, *J. Chem. Phys.*, **72**, 99.
[49] Bell, R. J., Dean, P. and Hibbins-Butler, D. C. (1970). Localization of normal modes in vitreous silica, germania and beryllium fluoride, *J. Phys. C: Solid St. Phys.*, **3**, 2111.

[50] Seeley, G. and Keyes, T. (1989). Normal-mode analysis of liquid-state dynamics, *J. Chem. Phys.*, **91**, 5581.
[51] Forrest, B. M., Leontidis, E. and Suter, U. W. (1996). A normal-mode study of a polymer glass containing a chromophore impurity, *J. Chem. Phys.*, **104**, 2401.
[52] Schober, H. R. and Laird, B. B. (1991). Localized low-frequency vibrational modes in glasses, *Phys. Rev. B*, **44**, 6746.
[53] Birch, J. R. (1992). The far-infrared optical constants of polypropylene, PTFE, and polystyrene, *Infrared Phys.*, **33**, 33.
[54] Guillet, J. (1985). *Polymer Photophysics and Photochemistry*, Cambridge: Cambridge University Press.
[55] Bailey, R. T., North, A. M. and Pethrick, R. A. (1981). *Molecular Motion in High Polymers*. Oxford University Press.
[56] Pant, P. V. K. and Boyd, R. H. (1993). Molecular dynamics simulation of diffusion of small penetrants in polymers, *Macromolecules*, **26**, 679.
[57] Bassolino-Klimas, D., Alper, H. E. and Stouch, T. R. (1993). Solute diffusion in lipid bilayer membranes: an atomic level study by molecular dynamics simulation, *Biochemistry*, **32**, 12624.
[58] Bassolino-Klimas, D., Alper, H. E. and Stouch, T. R. (1995). Mechanism of solute diffusion through lipid bilayer membranes by molecular dynamics simulation, *J. Am. Chem. Soc.*, **117**, 4118.